Corresponding Author: Mr. Ron Goldman, B.Sc.

Corresponding Author's Institution: Israel Oceanographic and Limnological Research

First Author: Ron Goldman, B.Sc.

Order of Authors: Ron Goldman, B.Sc.; Eli Biton; Eran Brokovich; Salit Kark; Noam Levin

Abstract: Recent gas discoveries in the eastern Mediterranean Sea led to multiple projects with substantial economic interest, and with them there is a risk of oil spills and their potential environmental impacts. To examine the potential spatial distribution of this threat, we created seasonal maps of the probability of oil spill pollution reaching an area in the Israeli coastal and exclusive economic zones, given knowledge of its initial sources. We performed simulations of virtual oil spills using realistic atmospheric and oceanic conditions. The resulting maps show dominance of the alongshore northerly current, which causes the high probability areas to be stretched parallel to the coast, increasing contamination probability downstream of source points. The seasonal westerly wind forcing determines how wide the high probability areas are, and may also restrict these to a small coastal region near source points. Seasonal variability in probability distribution, oil state, and pollution time is also discussed.

1
2
3
4
5
6
7
8
9
10
11
12
13
14
15
16
17
18
19
20
21
22
23
24
25
26
27
28
29
30
31
32
33
34
35
36
37
38
39
40
41
42
43
44
45
46
47
48
49
50
51
52
53
54
55
56
57
58
59
60
61
62
63
64
65

Oil spill contamination probability in the southeastern Levantine basin

Ron Goldman[a,*], Eli Biton[a], Eran Brokovich[b], Salit Kark[c], Noam Levin[b,d]

[a]*Israel Oceanographic and Limnological Research,31080 Haifa, Israel*
[b]*Department of Geography, The Hebrew University of Jerusalem, Mount Scopus, Jerusalem 91905, Israel*
[c]*The School of Biological Sciences ARC Centre of Excellence for Environmental Decisions (CEED), The University of Queensland, Brisbane, Queensland, Australia*
[d]*School of Geography, Planning and Environmental Management, Centre of Excellence for Environmental Decisions, The University of Queensland, Brisbane, Queensland, Australia*

Abstract

Recent gas discoveries in the eastern Mediterranean Sea led to multiple projects with substantial economic interest, and with them there is a risk of oil spills and their potential environmental impacts. To examine the potential spatial distribution of this threat, we created seasonal maps of the probability of oil spill pollution reaching an area in the Israeli coastal and exclusive economic zones, given knowledge of its initial sources. We performed simulations of virtual oil spills using realistic atmospheric and oceanic conditions. The resulting maps show dominance of the alongshore northerly current, which causes the high probability areas to be stretched parallel to the coast, increasing contamination probability downstream of source points. The seasonal westerly wind forcing determines how wide the high probability areas are, and may also restrict these to a small coastal region near source points. Seasonal variability in probability distribution, oil state, and pollution time is also discussed.

Keywords: simulation, oil spill, Eastern Mediterranean Sea, pollution, probability

1. Introduction

The infamous BP/Deepwater Horizon Oil and Gas Disaster in the Gulf of Mexico in 2010 (Norse and Amos, 2010) provides a notorious example for environmental damages that might result from oil and natural gas exploration and drilling activities. Oil and gas exploration and production have been established in several areas of the Mediterranean Sea for several decades(Belopolsky

---

*Corresponding author, Tel. +972-4-8565246
Email addresses: `ron@ocean.org.il` (Ron Goldman), `elib@ocean.org.il` (Eli Biton), `eran.brokovich@mail.huji.ac.il` (Eran Brokovich), `s.kark@uq.edu.au` (Salit Kark), `n.levin@uq.edu.au` (Noam Levin)

et al., 2012; Stocker, 2012). Exploration in the Nile Delta has moved from onshore to offshore areas in the 1980s, and technological advances have since enabled exploration and drilling to be used in deep waters, greatly enhancing the proven reserves of natural gas in the area. Given the unique biodiversity of the Mediterranean Sea, and the intensity of human activities in the Mediterranean, it is highly important to better understand the possible impacts of oil and natural gas activities.

As defined in the 1982 UN Convention on the Law of the Sea (UNCLOS), a coastal state has sovereign rights to explore and exploit, conserve and manage the natural resources in its Exclusive Economic Zone (EEZ) (Kwiatkowska, 1991). Under UNCLOS, the EEZ can extend to a maximum distance of 200 nautical miles from the country's baseline.

Following the discoveries of very large gas fields during 2009-2010 in the Israeli EEZ (Fig. 1) there has been an increase in oil and gas exploration and gas production activities (Shaffer, 2011; Ratner, 2011). This increase in offshore exploration and production activities brings new challenges to decision makers with regards to conservation efforts, marine safety, and environmental protection. With increased oil and gas operations activity there is also an obvious increase in the risk for oil or other hydrocarbon pollution. Modelling tools enable us to create high resolution probability estimates for regions that might be affected by oil pollution. The resulting probability maps are, therefore, extremely important to decision makers, when forming plans for marine protected areas, placing new infrastructures, or enacting protocols on handling marine pollutions.
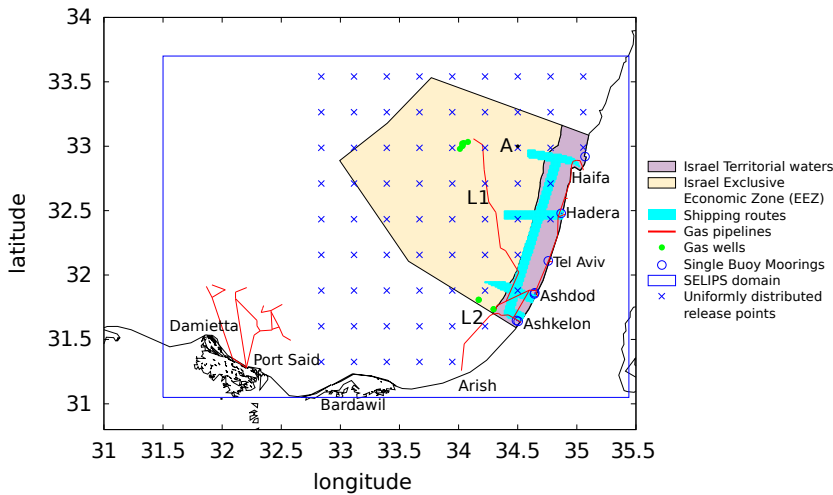

Figure 1: Infrastructure in the south eastern corner of the Mediterranean near Israel's proposed exclusive economic zone. L1: Tamar gas pipeline. L2: Arish-Ashkelon pipeline.

The use of numerical models to estimate the wind and ocean currents, which determine oil slick trajectories, has been growing in recent years: Some indi-

vidual oil spills events that have occurred in the Mediterranean Sea have been simulated (e.g. the Lebanon crisis oil spill in 2006 (Coppini et al., 2011)) and operational systems such as the Mediterranean Decision Support System for Marine Safety (MEDESS-4MS)(Zodiatis et al., 2012) make use of high resolution ocean forecast models to simulate new spills as they are reported. It is also common to simulate worst case oil spill scenarios for risk assessment.

The aims of this study are: (1) to estimate the location of regions in Israel's EEZ, having high probability of being contaminated by an oil slick. (2) to relate the spatial distribution of these regions to the initial position of the spill and to the synoptic state (atmospheric and oceanic conditions), so as to improve Israel's preparedness for the event of an oil spill. For this end, we produce statistical estimates of probability based on simulation of a large number of virtual oil spills which are transported by realistic wind and ocean currents. In that, we follow techniques similar to the ones which have been used in the gulf of Mexico by OSRA (Price et al., 2003), or in archipelago of La Maddalena, located in the northern extremity of Sardinia Island by Olita et al. (2012). Our work is also related to the work of Ferraro et al. (2009) who used radar based remote sensing of possible oil slicks to estimate the density of oil spills in the Mediterranean as well as in other European seas. However, their work was based on actual observations which were mapped over a much coarser resolution (1°) than the one used in our work.

The manuscript is ordered in the following way: In § 2 we review the main characteristics of the regional atmospheric and oceanographic circulations. In § 3 we briefly describe the numerical models used in simulating the oil spills and the calculation of oil pollution probabilities. In § 4 we present and discuss the probability estimates, their seasonality, and their relation to the weather and ocean circulation patterns. We conclude in § 5.

2. Regional Atmospheric and Oceanic Systems

2.1. Regional Meteorology

In our analysis of the results, we consider the following regional atmospheric and oceanic circulation patterns: The weather in the south eastern Mediterranean is characterized by 6 major synoptic systems (Alpert et al., 2004).

1. Cyprus lows - winter low pressure storms whose center travels east in the northern part of the basin. The winds southeast of the center are southerly to easterly winds whereas strong westerlies blow west of the cold front.
2. Persian trough is a persistent weather system during summer. It is characterized by westerly wind.
3. Red Sea trough (RST also known as Sudan trough) - this trough extends north from the Red Sea during the cold season. The axis of the trough separates the easterly wind east of it from the northerly wind west of it. The position of this axis, east or west of the coastline, greatly determines the coastal weather.

3

4. Sharav lows or khamsin lows, which are common in spring, are thermal low pressure systems whose center travels east along the southern coast of the Mediterranean. They induce easterly winds over the sea east of their center and north-westerly wind west of their center.

5. Siberian high, usually characterized by northerly winds along the Israeli coast.

6. Subtropical high usually characterized by calm weather.

2.2. Regional Ocean Circulation

A major feature in the circulation at the sea surface of the south-eastern Mediterranean Sea is a cyclonic along-slope current flowing over the shelf and slope areas (Rosentraub and Brenner, 2007). This current is persistent throughout most of the year though it may be interrupted by episodes of southward flow. Suggested causes of such episodes include strong easterly and northerly winds typical to the RST as well as influence of off-shelf anticyclonic eddies (Rosentraub and Brenner, 2007). The maximal velocity is usually attained during summer or during storm events (values as high as $1\,\mathrm{m/s}$ have been observed during winter (Rosentraub et al., 2010)). The meandering of the along-slope current has been shown to be related to the exchange of coastal and deep water in either the detachment of the anticyclonic Shikmona eddy near Haifa bay (Gertman et al., 2010) or the formation of filaments of coastal waters intruding to deep waters (Efrati et al., 2013). Beyond the slope area, the flow is not characterized by a single permanent feature, but rather by an area populated with dynamic meso-scale eddies (Amitai et al., 2010). The circulation on average in this area is anticyclonic, but can be locally interrupted by cyclonic mesoscale patterns. Particularly, the area between latitudes $33°\,\mathrm{N}$ and $35°\,\mathrm{N}$ and east of $32°\,\mathrm{E}$, which includes the Eratostenes sea-mount, is a known location of recurring anticyclonic eddies (Shikmona/Cyprus eddies). As discussed by Menna et al. (2012), this area can contain one or two eddies.

3. Methods

In this study we performed numerical simulations of oil spill events in order to estimate the probability of different areas being polluted by oil. We treated different scenarios, each characterized by the spill event's proximity to different possible sources of pollution, namely: shipping routes, pipelines, gas wells, single buoy moorings (SBM) and even distribution in space (Fig. 1). From each of these scenarios, a group of spill events was generated either randomly or evenly distributed. Ideally, the scenarios should account for all the possible synoptic weather and ocean current patterns which influence the trajectory of the oil slick. In practice we sampled the synoptic conditions by sampling the time of the initial spill from a year of atmospheric and ocean forecasts. Specifically, we used the SKIRON operational atmospheric forecasting system and SELIPS circulation forecasts from September 2012 to August 2013 to provide wind and currents to the MEDSLIK oil spill model. Cutting off at August was motivated

by the low variability in the atmospheric forcing during this time. We have not considered gas leaks, liquid natural gas spill or gas well blow-outs. We did this because the area affected by such events is expected to be relatively small (e.g., Hightower et al. (2004) recommend a hazard radius from liquid natural gas spill to be 2500 m) and the gas is expected to evaporate and disperse in the atmosphere quickly.

In subsections 3.1-3.2 we describe the atmospheric and oceanic models used. MEDSLIK is described in subsection 3.3. Subsection 3.4 describe how oil spill events were sampled and analysed.

3.1. Atmospheric Model - SKIRON

The SKIRON system has been developed by the Atmospheric Modeling and Weather Forecasting Group in the university of Athens (Kallos et al., 1997). SKIRON provides daily atmospheric forecasts with horizontal spatial resolution of $0.05°$ and temporal resolution of 1 hour. Wind fields of SKIRON are used within the MEDSLIK oil spill model whereas fields of wind, air temperature, mean sea level pressure, relative humidity, and incoming solar radiation are also used by the ocean circulation model to provide consistent ocean currents.

Wind roses derived from SKIRON wind field at point A of Fig. 1 can be seen in Fig. 2. North-westerly to south-westerly winds were common throughout most of the year. In summer and late spring these winds occurred due to the Persian trough, and during fall, winter, and early spring due to cold front of passing lows and due to subtropical highs. During winter and fall easterly winds were also common mostly due to warm front of Cyprus lows and Sharav lows, or as part of the RST. In Israel, the wet season of 2012-2013 had 53 rainy days, which is slightly below the average of 57 days. However, due to extreme storm events during November 2012 to January 2013, the total rainfall was slightly above average (107%) (IHS, 2013). This indicates that our estimates for the non-summer quadrants are more biased towards severe weather.

3.2. Oceanic Model - SELIPS

The South Eastern Levantine Israeli Prediction System (SELIPS) is a forecasting system, which is developed and operated by Israel Oceanographic and Limnological Research (IOLR). The System produces daily forecasts of temperature, salinity and sea currents in the south eastern corner of the Levantine Basin (the model domain can be seen in Fig. 1). The oceanic general model used to run SELIPS is the Princeton Ocean Model (POM)(Blumberg and Mellor, 1987). Model resolution is $0.01° \times 0.008\,33°$ with 27 sigma levels, the minimal depth is 5 m. Initial and boundary conditions of temperature, salinity, and water velocity for the oceanic model are provided through a one-way nesting of SELIPS in the ALERMO forecast system (Zafirakou-Koulouris et al., 2012). Atmospheric fluxes of heat, fresh water, and momentum at the sea surface are computed from bulk formulas using atmospheric forecasts of SKIRON. The model is initialized from the ALERMO first day forecasts datasets. The resulting temperature, salinity, velocity, and elevation fields are used to initialize POM for a two day
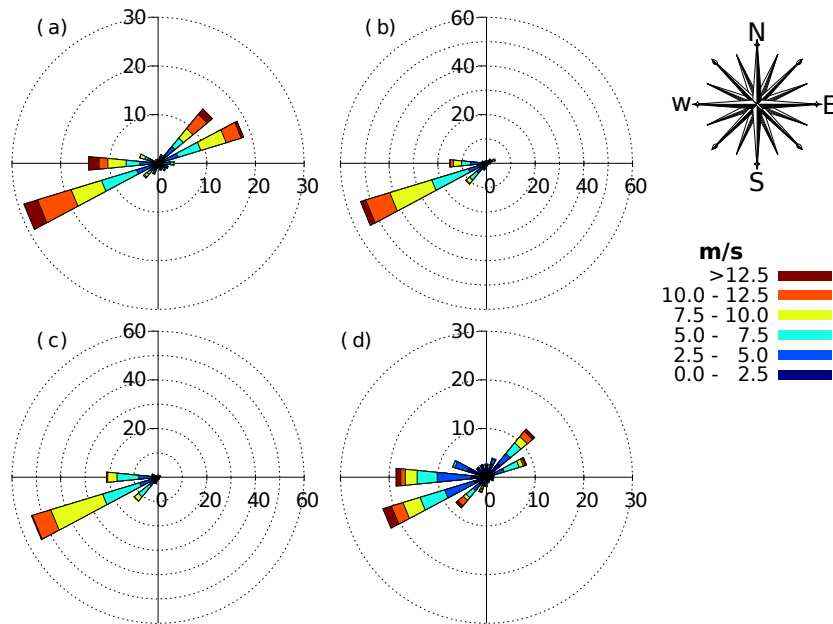
5

Figure 2: Seasonal wind roses at point A of Fig. 1 according to SKIRON forecasts. a: Winter (Jan-Mar 2013); b: Spring (Apr-Jun 2013); c: Summer (Jul-Aug 2013, Sep 2012); d: Fall (Oct - Dec 2012). Bar direction indicates the direction from which the wind is blowing.

hindcast run in which the heat flux is corrected through nudging by remotely sensed sea surface temperature (SST) fields. The averaged fields of the last day of the hindcast are used as initial condition to the forecast. The dataset used in MEDSLIK is built by concatenating the first forecast day in the form of 6-hour averaged fields of SST and currents interpolated to fixed depths of 0 m, 10 m, 30 m, 120 m, 300 m, 600 m, 1000 m, 1500 m and 2000 m.

The seasonal average of the SELIPS current field at the upper sea layer is displayed in Fig. 3. One can see the existence of the alongshore current during winter and summer. The average alongshore current during summer was narrower and stronger than during winter. During fall and spring the average current was much weaker due to more events of southerly current and weaker northerly current.

The dataset, compared with SST, has a warm bias of 0.088 °C and RMS error of 0.603 °C in the domain of interest. the north of the model suffers from a cold bias and as a results, high pointwise RMS. Visual comparison of simulated flow patterns with satellite chlorophyll images suggests that the model is capable of recreating the along-slope current. Sub basin scale eddies, as well as mesoscale features such as shelf water filaments formation and eddy detachments, are created by the model but were often in the wrong position or were in disagreement with chlorophyll patterns. Our comparisons therefore indicates that the dataset created by the model is realistic, not in the sense that
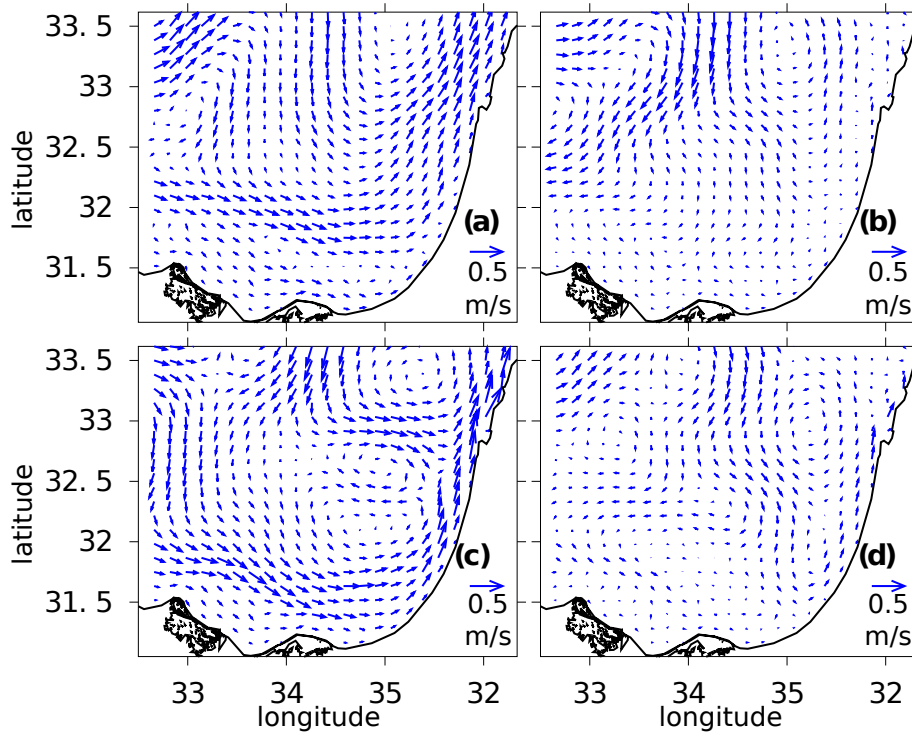
6

Figure 3: Seasonally averaged currents from SELIPS forecasts. a: Winter (Jan-Mar 2013); b: Spring (Apr-Jun 2013); c: Summer (Jul-Aug 2013, Sep 2012); d: Fall (Oct - Dec 2012).

it accurately portray the flow field from September 2012 to August 2013, but in that it exhibits the permanent and seasonal features of the circulation, as well as possible subbasin and mesoscale features.

3.3. MEDSLIK

MEDSLIK (Lardner, 2009) is a program, which simulates the propagation and fate of an oil slicks using a 3D Monte Carlo method by calculating the trajectory and evolution of hundreds of small oil parcels for each oil slick. Each parcel is transported according to the wind and currents in addition to a random walk process which simulates the oil slick diffusion. Oil evaporation, emulsification, mixing, and beaching are also taken into account. At output times, the parcels are collected in bins according to their location and separated according to their state (i.e. if the oil exists as surface layer, as an emulsion of water and oil within the water column, or if the oil is beached). MEDSLIK has been integrated to the Mediterranean Decision Support System for Marine Safety (MEDESS-4MS) and is also currently used to assist the Israeli Ministry of Environmental Protection in case of oil pollution.

7

3.4. Oil Spill Simulations

Each spill scenario (a group of oil spill releases near pipelines; ship routes; single buoy moorings; gas wells) was simulated separately. Conditional probability maps were calculated for each scenario as described below. In addition, a scenario representing a spatially uniform distribution of oil spills in deep water was also treated in order to examine the effects of wind and ocean currents on the conditional probability while mitigating the effect of the local initial source distribution. We did not treat scenario of spills inside ports or from inland infrastructure. The percentage of oil that is immediately beached in such events is very sensitive to the choice of the point were the oil is released. Each spill event was simulated separately as an event in which oil is released instantaneously at a specific point and then flows for 10 days. Simulation longer than 10 days resulted in no significant changes to the conditional probability maps. The location of the oil slick was extracted every 3 hours and re-sampled from a grid with bins of size $300\,\mathrm{m} \times 300\,\mathrm{m}$ to a uniform global grid with bin size of $1\,\mathrm{km} \times 1\,\mathrm{km}$. This grid was set in the region south of $33.2°\,\mathrm{N}$ and east of $32.5°\,\mathrm{E}$. Trimming the domain reduced the problems associated to the boundaries of SELIPS, which include inaccurate currents close to the boundary and the problem of slicks, which leave the domain but should or should not return to it when currents and wind change direction.

The conditional probability $P_E(x,y)$ of a bin centred at longitude x and latitude y being contaminated, given a spill event in the scenario E, was estimated as the number of simulations, in the scenario corresponding to E, in which the bin was contaminated (at any time during the 10 day simulation), divided by the total number of simulations in that scenario. In order to examine the seasonal changes in conditional probability, we have subdivided the scenarios according to the date of initial spills. The date groups are a) winter: January to March, b) spring: April to June, c) summer: July to September and d) fall: October to December. The subscript E, denoting the scenario, is one of S, P, W, M, U to indicates source near shipping routes, pipelines, gas wells, single buoy moorings (SBM), or uniformly distributed grid, respectively.

Formally, if $C(x,y,t,\omega)$ is the concentration of oil at a bin centred at longitude x and latitude y at time step $t = 0\,\mathrm{h}, 3\,\mathrm{h}, \dots, 240\,\mathrm{h}$ resulting from oil spill event ω, then a pollution indicator is defined as:

$$I(x,y,T,\omega) = \left\{ \begin{array}{ll} 1 & max\{C(x,y,t,\omega) : t < T\} > 0 \\ 0 & otherwise \end{array} \right. , \qquad (1)$$

and conditional probability was estimated as:

$$P_E(x,y,T) = \frac{\sum_{\omega \in E} I(x,y,T,\omega)}{\sum_{\omega \in E} 1}. \qquad (2)$$

We denoted $P_E(x,y) \doteq P_E(x,y,240\,\mathrm{h})$ as the conditional probability of being contaminated within 10 day from the initial release.

8

Mean pollution time was estimated as the average total time in which an area is polluted during a simulation:

$$\tau(x,y) = \frac{\sum_{\omega \in E} \sum_{t=0\,\mathrm{h}}^{240\,\mathrm{h}} I(x,y,t,\omega) \cdot 3\,\mathrm{h}}{\sum_{\omega \in E} I(x,y,240\,\mathrm{h},\omega)} \qquad (3)$$

The average is taken over simulations in which the bin is polluted, thus "highlighting" areas of low conditional probability. The mean time is obviously influenced by the speed of the slick, but also from the shape of the oil slick (e.g. an elliptical slick travelling along its major axis will produce longer pollution time than a circular slick having the same area and travelling at the same speed). This analysis is less effective when considering areas where slick are still travelling through by the end of the simulations. τ values in such area are biased toward short pollution time compared with upstream areas. In scenarios containing spatially separated sources (e.g. the pipeline scenario where slicks arrive from Israeli pipelines and from Egyptian pipelines), τ values may have a bimodal distribution due to differences in travel time from the different sources.

Oil spill events near pipelines and shipping routes were sampled randomly in space and time to better account for the complex spatial structure and to give better resolution to these important source points. The shipping route ensemble had 12000 simulations and the pipeline ensemble 3600. The uniform distribution in ensemble U had 4896 simulations with spacing of 0.277° between grid points (Fig. 1) and 5 days intervals between events. This was done since the entire model domain was too large to be evenly sampled by random distribution. Point data (i.e., SBM and gas wells) was also sampled evenly in time (i.e., every 5 days). We have seen in sensitivity tests that the distribution pattern of the estimated conditional probability did not change significantly when spill volume was changed, we therefore, chose not to sample over different spill volumes but to use a single instantaneous spill volume of 100 t. Additionally, we have chosen not to sample over different specific gravity values (prescribed to MEDSLIK as American Petroleum Institute gravity, or API gravity) and used a single value of API gravity 42, which is the API gravity of light fuel (petroleum liquids with an API gravity greater than 10 float on water).

4. Results and Discussion

The dominance of the along shore current is clearly seen in maps of the conditional probability estimates (Fig. 4-Fig. 7). The effect is noticed in the fact that areas of high conditional probability were elongated parallel to the current and are located somewhat downstream from their source area (e.g., Fig. 4, Fig. 5c, and Fig. 7c). Additionally, release areas which were oriented along the coast created areas of higher probability than release areas which were oriented across it (Fig. 4, Fig. 8). This occurred because oil slicks that are oriented along the coasttravelled along similar or overlapping trajectories, thus increasing their conditional probability estimate, whereas oil slicks released
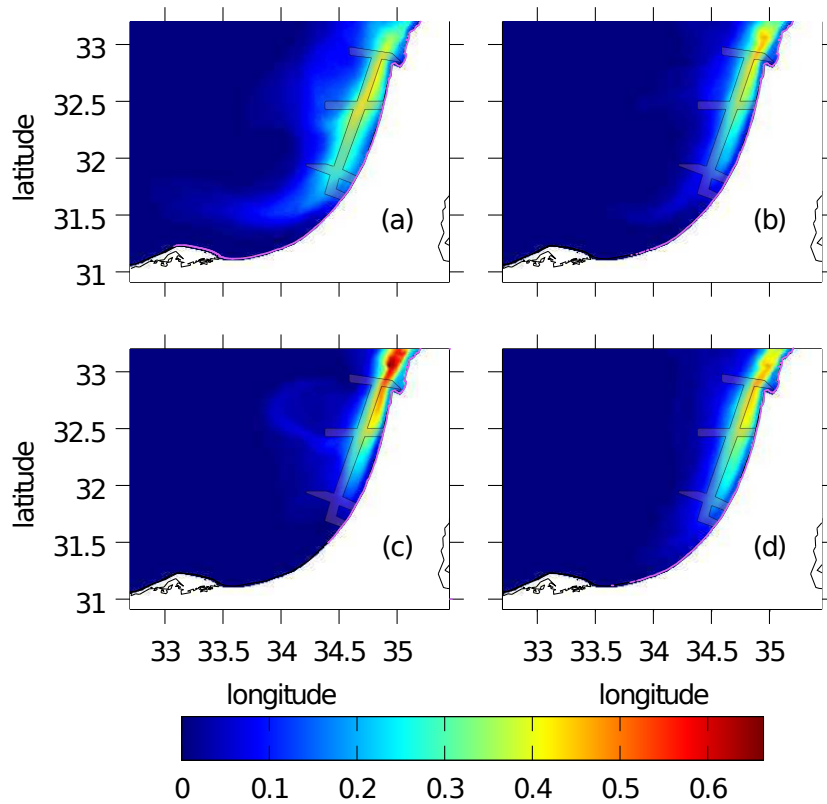
9

Figure 4: Seasonal conditional probability for contamination of bin (x, y) given a spill released at the ship route area based on 10 days of simulation ($P_S(x, y)$). Spills start during a: Winter (Jan-Mar 2013); b: Spring (Apr-Jun 2013); c: Summer (Jul-Aug 2013, Sep 2012); d: Fall (Oct - Dec 2012). purple line indicate locations where beaching occurred.

in areas that are oriented perpendicularly to the coasttravelled in trajectories which were parallel to one another. This effect is more apparent when one examines, for example, the conditional probability from spills near pipelines, derived based only on the first day of the simulation i.e., $P_P(x, y, 24\,\text{h})$ (Fig. 9): Slicks originating from the Tamar pipeline (L1 in Fig. 1) were scattered almost perpendicularly to the pipeline whereas slicks originating near the midsection of Arish-Ashquelon pipeline (L2 in Fig. 1) travelled parallel to it. One should note, that the conditional probability values in Fig. 9 (0.045 maximum) are smaller than in Fig. 8 (0.2 maximum) since the slick trajectories were shorter and did not yet overlap each other.

The conditional probability maps vary with the seasons. Generally, during winter larger areas had non-zero probability than in summer. This is most evident when regarding the mooring points (Fig. 6): In spring and summer the slicks were pushed toward the coast, most likely by the westerly wind, and only the nearby coastal area was affected. This did not occur during winter and fall,

10
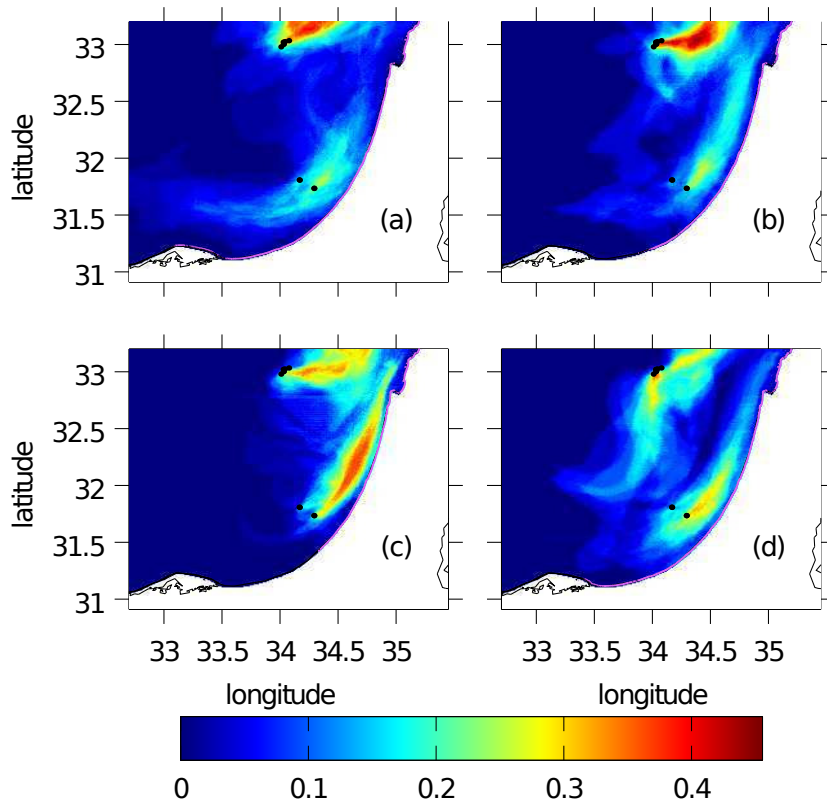
Figure 5: Same as in Fig. 4, but for $P_W(x, y)$ i.e., spills released near gas wells.

and therefore a much larger area was at risk, including deep water as well as coasts away from the spills. Another feature, which influenced the conditional probability pattern, was the existence of anti-cyclonic eddy south west of Haifa bay (33.5° E- 34.5° E, 32.4° N-33° N) during summer (Fig. 3c). Slicks whose origin lied inside the eddy remained within it, and some of the slicks whose origin was at the western side of the alongshore current south of the eddy also entered the eddy domain and flew inside it. In this manner, the conditional probability of pollution of the eddy domain increased (Fig. 4c, Fig. 8c, and Fig. 7c). Because most origin points were located in the alongshore current, the eddy features have not dominated the conditional probability field except in the case of $P_U(x, y)$ (Fig. 7c), where most origin point were located away from the coast.

A recurring feature of the conditional probability distribution pattern is a thin strip (reaching a width of 10 km) of relatively low conditional probability, which lies between the coast and the elongated areas of high conditional probability (e.g., Fig. 4, Fig. 8, Fig. 7). Two possible explanations for this phenomenon are: First, since the velocity at the coast was zero, there was a coastal

11
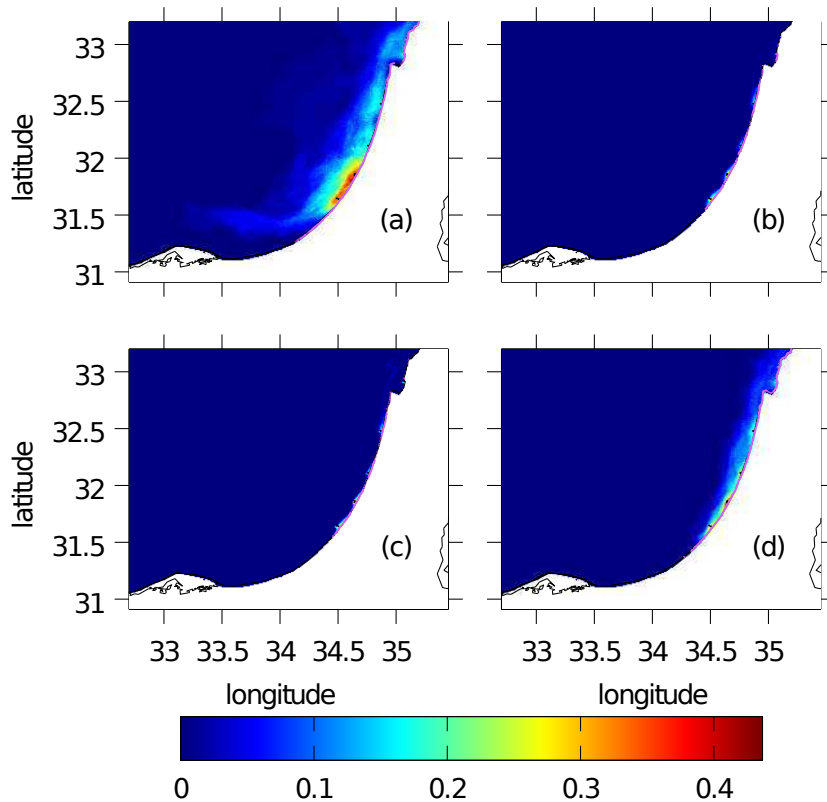
Figure 6: Same as in Fig. 4, but for $P_M(x, y)$ i.e., spills released near SBM.

boundary layer in which the current was almost entirely parallel to the coastline and the velocity was reduced. This boundary layer reduced the amount of oil parcels which reached the shore, and therefore, reduced the conditional probability in that layer. Second, oil parcels which did transverse the boundary layer had a good chance of being deposited on the shore or on the bottom of the sea and could not travel further to pollute other areas.

Fig. 10 overlays mean pollution time maps with contours of the conditional probability for the ship route scenario (calculations in other scenarios had provided similar results and, therefore, are not shown). The mean pollution time, τ, in the alongshore current varies along the coast from season to season. During winter, spring and fall, pollution time along the Israeli coast is longer than in summer. Moreover, high τ values are located in an elongated region, which during wind winter, is slightly shifted coast-ward from the maximal conditional probability. There is a thin strip separating the offshore maximal τ values from the coastal maximal τ. The existence of the maximal τ region in the alongshore current is most likely due to elongation of the slicks parallel to the flow (Haller and Yuan, 2000). However, events of southerly current, in which north-

12
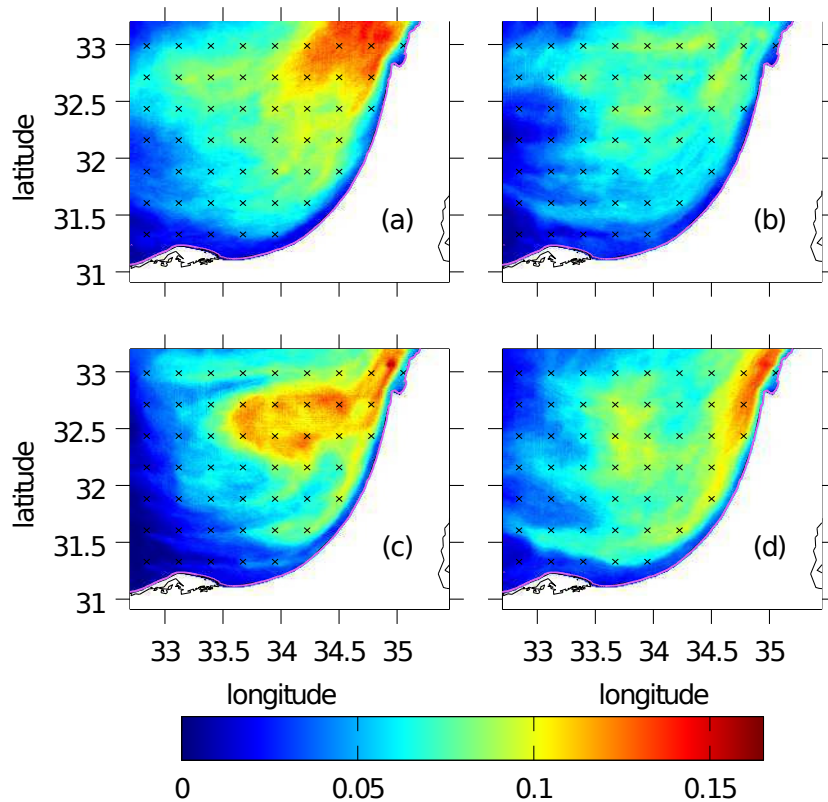
Figure 7: Same as in Fig. 4, but for $P_U(x, y)$ i.e., spills released from an uniformly distributed grid.

ward motion is intermitted with southward motion, may further increase the pollution time. the coast-ward shift of maximal τ may be attributed to the shear of the coastal boundary layer (i.e. to lower current velocities closer to the shelf). The existence of the low-τ strip (whose width is similar to the low probability strip) suggests that during these seasons the two mechanisms discussed previously for reducing probability on the shelf and slope (i.e. beaching and the coastal boundary layer), are dominant in different areas, with oil beaching being more dominant at the thin low probability strip, and the coastal boundary layer, characterized by shear, being more dominant further offshore. During summer the alongshore strip of maximal τ exists, but values are smaller and the strip is almost indistinct. This may be a results of having a strong, permanent northerly current with a much smaller boundary layer, as evident in Fig. 3c.

Away from the along-shore current, areas of high pollution time occur where the currents are weak (e.g. in centres of eddies and near saddle points in the flow), however the conditional probability of those areas being polluted was very low.

13
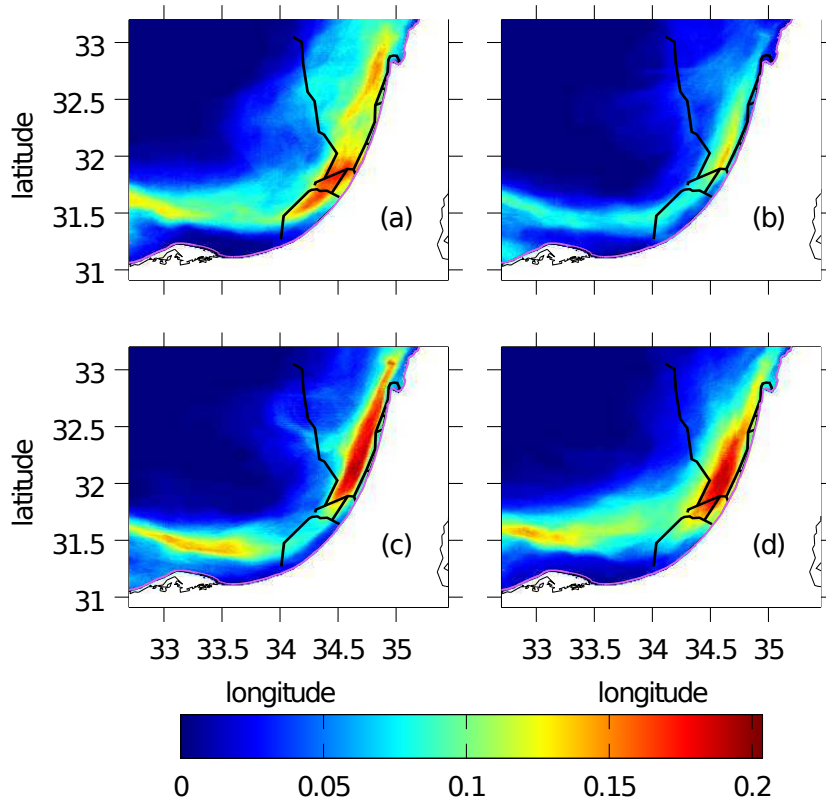
Figure 8: Same as in Fig. 4, but for $P_P(x, y)$ i.e., spills released near pipelines.

Fig. 11 shows the oil state at the end of the run in the ship route scenario. The amount of evaporated oil after 10 days was constant (55.8 %). The rest of the oil exist as surface oil, beached oil, dispersed oil in the water or precipitated on the bottom (not available as output from MEDSLIK). Our choice of API gravity meant that the majority of the oil parcels in the water will be in a state of either surface oil or beached surface oil. The resulting trade-off between surface and beached oil is exhibited in Fig. 11. Events states were clustered either near complete beaching or no beaching. The trade-off between oil dispersed in the water column, and the total of beached and surface oil is much milder. Seasonality is evident in the amount of oil dispersed in the water column with high percentages in winter and fall and low in summer. Based on Fig. 11 we may estimate the frequency of severe beaching in each scenario as the percent of simulations in which more than 35 % of of the oil is beached (Table 1). The amount of beaching varies greatly depending on scenario but also according to the seasons. Severe beaching is more common in the fall and spring compared to summer and winter. This is most likely due to weakening of the alongshore current and the boundary layer caused by it during fall and spring, making the
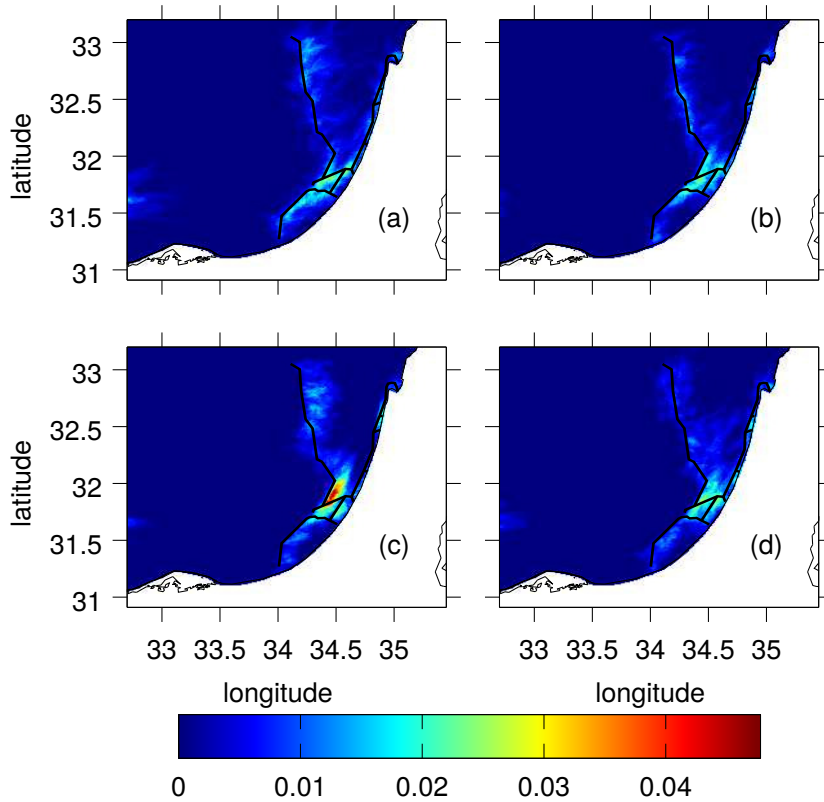
14

Figure 9: Seasonal conditional probability for contamination of bin (x, y) given a spill released near pipelines based on 1 day of simulation ($P_P(x, y, 24\,\mathrm{h})$). Spills start during a: Winter (Jan-Mar 2013); b: Spring (Apr-Jun 2013); c: Summer (Jul-Aug 2013, Sep 2012); d: Fall (Oct - Dec 2012).

wind more dominant in determining the slick trajectory.

The conditional probability for pollution in beaching at coastal area can be inferred, for each scenario, from Fig. 4-Fig. 8. In the ship scenario, relatively higher values exist between Hadera and Haifa all year, in the southern coasts during winter and fall, and in Haifa bay and the northern coast during summer (Fig. 4). In the SBM scenario, coastal high values areas are located upstream close to the SBM during summer and spring but spread during winter and fall (Fig. 6). The pipeline scenario has high values along the entire Israeli coast with a local minima south of Hadera and from Haifa bay north (Fig. 8). the evenly distributed grid scenario has relativly even distribution on the coast with a slight maximum between Hadera and Haifa. the gas well scenario has higher values between Ashdod and Haifa during summer, south of Tel-Aviv during winter and fall and even values during spring (Fig. 5).

15
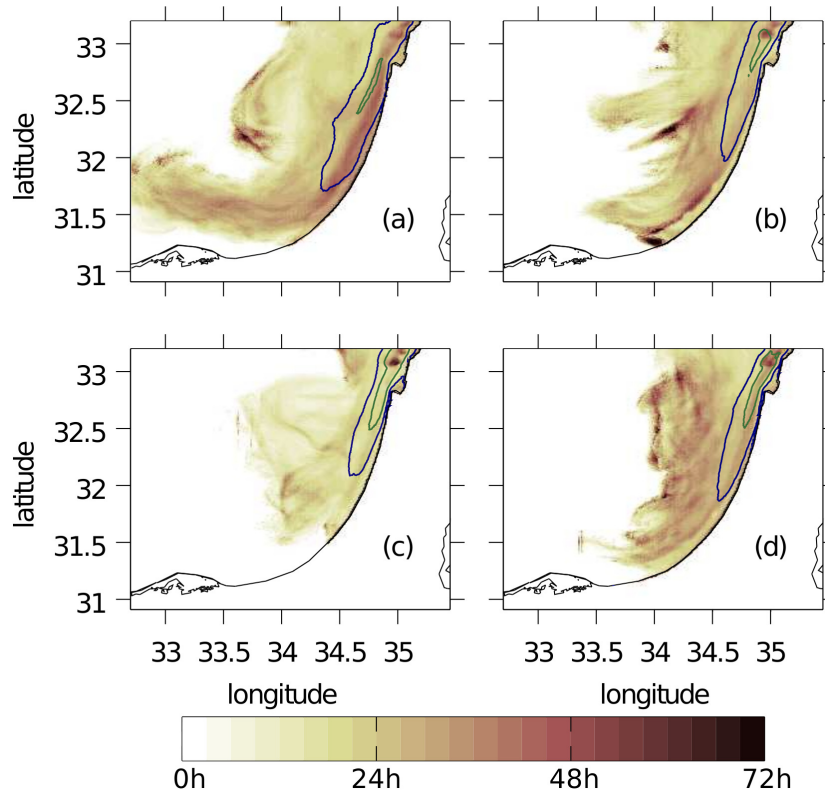
Figure 10: Mean pollution time τ for the ship route scenario. Contours of conditional probability $P_S = 0.2$ (blue) and $P_S = 0.4$ (green) are given for reference. Spills start during a: Winter (Jan-Mar 2013); b: Spring (Apr-Jun 2013); c: Summer (Jul-Aug 2013, Sep 2012); d: Fall (Oct - Dec 2012).

16

scenario	winter	spring	summer	fall
ship routes	66	75	63	79
even grid	22	30	28	34
gas wells	23	35	37	35
SBM	95	100	100	100
pipelines	56	70	66	73

Table 1: Percentage of simulations where more than 35 % of the oil is beached.

5. Conclusions

In this study we performed numerical simulations of oil spill events in Israel's Mediterranean Sea region, in order to estimate the conditional probability of different areas being polluted by oil, given that the origin of the spill is close to shipping routes, pipelines, gas wells and single buoy moorings. The simulations were carried out using the MEDSLIK oil spill model using realistic synoptic conditions by sampling the time of the initial spill from one year of atmospheric and ocean forecasts. Our results exhibited the strong influence of circulation patterns (in particular the alongshore current) and seasonality on probability estimates.

Systematic conservation planning involves the definition of quantitative goals for conserving biodiversity features (e.g., area required for ensuring the persistence of a specific species or habitat), and the identification of priority areas that succeed in maximizing the achievement of conservation goals while minimizing threats or costs (Margules et al., 2002). The outputs of the simulations developed in this study, can inform the process of systematic conservation planning. Oil spill contamination probabilities can be incorporated as a risk to certain species, depending on their distribution range area. Threats to biodiversity can be explicitly included within prioritization software (Game et al., 2008) as can be done using a modified version of Marxan systematic reserve planning software called Marxan with Probability (MarProb) (Tulloch et al., 2013), aiming to create marine protected areas where the risks are lower.

Future studies may use more realistic scenarios. Improvements include better mapping of ship routes (see Halpern et al. (2008) and Wang et al. (2008) regarding spatial datasets of shipping tracks and their limitations); considering offshore platforms and shipping in the upstream area of the Nile Delta; accounting for spill size and type; applying threshold values to concentrations appearing in (1); using more than one year of weather and ocean circulations to get better statistics of the synoptic states; and considering events of non instantaneous spills near wells, pipes and SBM. Estimating the probability of scenario occurrence is also of great importance. Especially in cases where one is interested in the probability of an area being contaminated by oil but not in the source of the pollution.

acknowledgement
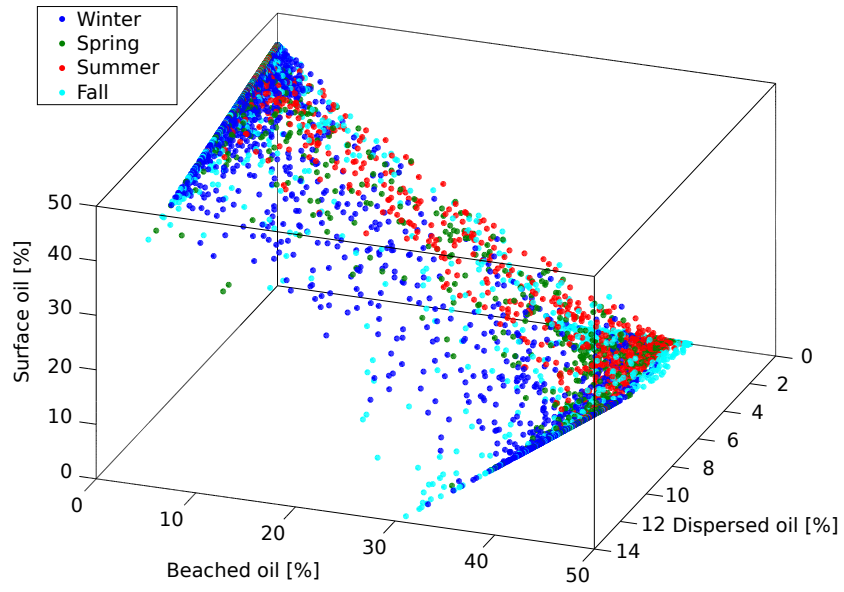
Figure 11: Oil state in the entire oil slick after 10 days. Each dot represents an oil spill event from the ship route scenario.

19

References

Alpert, P., Osetinsky, I., Ziv, B., Shafir, H., 2004. Semi-objective classification for daily synoptic systems: application to the eastern Mediterranean climate change. Int. J. Climatol. 24, 1001–1011. doi:10.1002/joc.1036.

Amitai, Y., Lehahn, Y., Lazar, A., Heifetz, E., 2010. Surface circulation of the eastern Mediterranean Levantine basin: Insights from analyzing 14 years of satellite altimetry data. J. Geophys. Res. Oceans 115. doi:10.1029/2010JC006147.

Belopolsky, A., Tari, G., Craig, J., Iliffe, J., 2012. New and emerging plays in the Eastern Mediterranean: an introduction. Pet. Geosci. 18, 371–372. doi:10.1144/petgeo2011-096.

Blumberg, A.F., Mellor, G.L., 1987. A Description of a Three-Dimensional Coastal Ocean Circulation Model. American Geophysical Union. pp. 1–16. doi:10.1029/CO004p0001.

Coppini, G., Dominicis, M.D., Zodiatis, G., Lardner, R., Pinardi, N., Santoleri, R., Colella, S., Bignami, F., Hayes, D.R., Soloviev, D., Georgiou, G., Kallos, G., 2011. Hindcast of oil-spill pollution during the Lebanon crisis in the Eastern Mediterranean, July−August 2006. Mar. Pollut. Bull. 62, 140 – 153. doi:10.1016/j.marpolbul.2010.08.021.

Efrati, S., Lehahn, Y., Rahav, E., Kress, N., Herut, B., Gertman, I., Goldman, R., Ozer, T., Lazar, M., Heifetz, E., 2013. Intrusion of coastal waters into the pelagic eastern Mediterranean: In situ and satellite-based characterization. Biogeosciences 10, 3349–3357. doi:10.5194/bg-10-3349-2013.

Ferraro, G., Meyer Roux, S., Muellenhoff, O., Pavliha, M., Svetak, J., Tarchi, D., Topouzelis, K., 2009. Long term monitoring of oil spills in European seas. Int. J. Remote Sens. 30, 627–645. doi:10.1080/01431160802339464.

Game, E.T., Watts, M.E., Wooldridge, S., Possingham, H.P., 2008. Planning for persistence in marine reserves: a question of catastrophic importance. Ecol. Appl. 18, 670–680.

Gertman, I., Goldman, R., Rosentraub, Z., Ozer, T., Zodiatis, G., Hayes, D.R., Poulain, P.M., 2010. Generation Shikmona anticyclonic eddy from long shore current, in: Rapp. Comm. int. Mer Medit., p. 114.

Haller, G., Yuan, G., 2000. Lagrangian coherent structures and mixing in two-dimensional turbulence. Physica D 147, 352 – 370. doi:10.1016/S0167-2789(00)00142-1.

Halpern, B.S., Walbridge, S., Selkoe, K.A., Kappel, C.V., Micheli, F., D'Agrosa, C., Bruno, J.F., Casey, K.S., Ebert, C., Fox, H.E., Fujita, R., Heinemann, D., Lenihan, H.S., Madin, E.M.P., Perry, M.T., Selig, E.R., Spalding, M., Steneck, R., Watson, R., 2008. A global map of human impact on marine ecosystems. Science 319, 948–952. doi:10.1126/science.1149345.

Hightower, M., Gritzo, L., Luketa-Hanlin, A., Covan, J., Tieszen, S., Wellman, G., Irwin, M., Kaneshige, M., Melof, B., Morrow, C., Ragland, D., 2004. Guidance on Risk Analysis and Safety Implications of a Large Liquefied Natural Gas (LNG) Spill Over Water. Technical Report. Sandia National Laboratories Albuquerque NM.

IHS, 2013. Summary of the 2012/13 Rain Year, Hydrological Charectaristics. Technical Report. The Governmental Authority for Water and Sewage. Jerusalem, Israel. In Hebrew.

Kallos, G., Nickovic, S., Papadopoulos, A., Jovic, D., Kakaliagou, O., Misirlis, N., Boukas, L., Mimikou, N., Sakellaridis, G., Papageorgiou, J., 1997. The regional weather forecasting system SKIRON: An overview, in: Proceedings of the symposium on regional weather prediction on parallel computer environments, p. 17.

Kwiatkowska, B., 1991. Creeping jurisdiction beyond 200 miles in the light of the 1982 law of the sea convention and state practice. Ocean Development & International Law 22, 153–187. doi:10.1080/00908329109545954.

Lardner, R., 2009. Medslik v. 5.3.1 User Manual. Oceanography center, University of Cyprus.

Margules, C., Pressey, R., Williams, P., 2002. Representing biodiversity: Data and procedures for identifying priority areas for conservation. J. Biosci. 27, 309–326. doi:10.1007/BF02704962.

Menna, M., Poulain, P.M., Zodiatis, G., Gertman, I., 2012. On the surface circulation of the Levantine sub-basin derived from Lagrangian drifters and satellite altimetry data. Deep Sea Res. Part I 65, 46 – 58. doi:10.1016/j.dsr.2012.02.008.

Norse, E.A., Amos, J., 2010. Impacts, perception, and policy implications of the BP/Deepwater Horizon oil and gas disaster. Environmental Law Reporter 40, 11058–11073.

Olita, A., Cucco, A., Simeone, S., Ribotti, A., Fazioli, L., Sorgente, B., Sorgente, R., 2012. Oil spill hazard and risk assessment for the shorelines of a Mediterranean coastal archipelago. Ocean Coast. Manage. 57, 44 – 52. doi:10.1016/j.ocecoaman.2011.11.006.

Price, J.M., Johnson, W.R., Marshall, C.F., Ji, Z.G., Rainey, G.B., 2003. Overview of the Oil Spill Risk Analysis (OSRA) model for environmental impact assessment. Spill Sci. Technol. Bull. 8, 529 – 533. doi:10.1016/S1353-2561(03)00003-3.

Ratner, M., 2011. Israel's Offshore Natural Gas Discoveries Enhance Its Economic and Energy Outlook. Technical Report.

Rosentraub, Z., Anis, A., Goldman, R., 2010. Wintertime cross shelf circulation and shelf/slope interaction off the central israeli coast, in: Rapp. Comm. int. Mer Medit., p. 171.

Rosentraub, Z., Brenner, S., 2007. Circulation over the southeastern continental shelf and slope of the Mediterranean Sea: Direct current measurements, winds, and numerical model simulations. J. Geophys. Res. Oceans 112. doi:10.1029/2006JC003775.

Shaffer, B., 2011. Israel-New natural gas producer in the Mediterranean. Energy Policy 39, 5379 – 5387. doi:10.1016/j.enpol.2011.05.026.

Stocker, J., 2012. No EEZ solution: The politics of oil and gas in the Eastern Mediterranean. The Middle East Journal 66, 579–597.

Tulloch, V.J., Possingham, H.P., Jupiter, S.D., Roelfsema, C., Tulloch, A.I., Klein, C.J., 2013. Incorporating uncertainty associated with habitat data in marine reserve design. Biol. Conserv. 162, 41 – 51. doi:10.1016/j.biocon.2013.03.003.

Wang, C., Corbett, J.J., Firestone, J., 2008. Improving spatial representation of global ship emissions inventories. Environ. Sci. Technol. 42, 193–199. doi:10.1021/es0700799.

Zafirakou-Koulouris, A., Koutitas, C., Sofianos, S., Mantziafou, A., Tzali, M., Dermissi, S.C., 2012. Oil spill dispersion forecasting with the aid of a 3D simulation model. J. Phys. Sci. Appl. 10, 448 – 453.

Zodiatis, G., Lardner, R., Solovyov, D., Panayidou, X., De Dominicis, M., 2012. Predictions for oil slicks detected from satellite images using MyOcean forecasting data. Ocean Sci. 8, 1105 – 1115. doi:10.5194/os-8-1105-2012.